

Electrochemically Deposited Bismuth-Telluride nanowires in nanoporous alumina membranes

M. Elyaagoubi^{1,2}, Y. Najih¹, M. Khadiri², M. Mabrouki^{1*}, A. Oueriagli², A. Outzourhit²

(1) Laboratoire de Génie Industriel FST Béni-Mellal, BP 523, 23000 Maroc

(2) Laboratoire de Physique du Solide et des Couches Minces (LPSCM) Faculté des Sciences Semlalia Marrakech, Maroc, Université Cadi Ayyad, BP 2390, Maroc

Received 02 Feb 2016,

Revised 19 May 2016,

Accepted 25 Sep 2016

Keywords

- ✓ Nanoporous alumina;
- ✓ Electrodeposition;
- ✓ Bismuth
- ✓ telluride;
- ✓ Nanowires.

mus_mabrouki@yahoo.com

Tel.: 0662012642.

Abstract

Bismuth Telluride nanowires were electrochemically deposited from solutions of Bi₂O₃ and TeO₂ in 1M HNO₃/dimethyl sulfoxide (DMSO) (50% v/v) onto nanoporous anodized aluminum oxide (AAO) films working electrodes at room temperature. A conventional three-electrode cell was used with a platinum sheet counter electrode and a saturated calomel reference electrode (SCE). The Bi-Te nanowires were prepared using potentials varying from -250 to -100 mV (versus SCE). X-ray diffraction (XRD) and scanning electron microscopy (SEM) were employed to characterize the nanowires. The XRD revealed that the deposit nanowires consist of Bi₂Te₃ Rhombohedral phase. SEM studies showed that the nanowires are homogeneous and may protrude from the anodized alumina nanopores depending on the deposition time as can be readily revealed by the current-time characteristics of the process.

1. Introduction

Bismuth telluride (Bi₂Te₃) and its doped derivative compounds are attracting strong research interest because of their excellent thermoelectric refrigeration characteristics for room temperature applications [1]. Bi₂Te₃ is a V–VI binary chalcogenide compound semiconductor, which can be tailored for n- and p-type conductivities by adjusting the composition [2]. Bismuth telluride (Bi₂Te₃)-containing alloys can be used for various applications including photovoltaic solar cells, thermoelectric devices, and infrared sensors [3–6].

The figure of merit of thermoelectric materials is given by $Z = \alpha^2 \sigma / \kappa$ where α is the Seebeck coefficient, σ is the electric conductivity and κ is the thermal conductivity of the material. Recent theoretical calculations have indicated that Z , or the dimensionless factor, ZT , where T is the absolute temperature, could be significantly improved by using 1D or 2D nanostructures to decrease the thermal conductivity by enhancing the phonon scattering effects [7, 8]. Several methods for preparing Bi₂Te₃ have been reported, including directional crystallization [9, 10], vacuum evaporation [11, 12], mechanical alloying [13], and spark plasma sintering [14]. Electrodeposition has also been reported for the preparation of Bi₂Te₃ [15–20].

Several growth techniques were proposed and used for fabricating 1D bismuth telluride (Bi₂Te₃) structures including template methods [21–24]. As a general principle, they consist in filling of the pores of a template matrix with the material of choice. Several techniques for pore filling were proposed: chemical vapor deposition [25] and electrochemical deposition [26–30]. Electrodeposition has proven to be a low-cost and high-yield technique for producing large arrays of nanowires or nanotubes. Possible templates include nuclear track-etched polycarbonate membranes, nanochannels array glasses, mesoporous channel hosts, and self-ordered anodized aluminum oxide (AAO) membranes. AAO is stable at high temperature and in organic solvents, and the pore channels in AAO are uniform, parallel, and perpendicular to the membrane surface [31–33].

The method we used is based on electrodeposition into the nanopores of AAO template using a 1M HNO₃ /dimethyl sulfoxide ((DMSO) (50% v/v) solution containing metal ions. The mixture of water / (DMSO) was used as an alternative to water, since it provides a wider electrochemical window for Bi₂Te₃ electrodeposition using Te and Bi salts. This expanded potential window allows for the use of more negative potentials without reduction of the solvent, thus preventing the formation of H₂ bubbles.

Moreover, because DMSO has a significantly higher viscosity compared to water, thus slowing down mass transfer to the bottom of the pores and is less corrosive, it is suitable for nanowires array deposition in porous alumina templates.

2. Experimental techniques

2.1. Preparation of alumina templates

Aluminum sheets of 2 mm in thickness were ultrasonically cleaned in acetone, rinsed with deionized water and then annealed at 400°C for 3 hours in vacuum to reduce mechanical stress in these substrates. They were subsequently electropolished in a mixture of perchloric acid and ethanol (1:4 v/v HClO₄: EtOH) at constant voltage of approximately 20 Volts and for 3 minutes at room temperature. The cleaned aluminum sheets were then used as the anode and a Platinum (Pt) foil as the cathode in the anodization cell. The first anodization was carried out in 0.3 M oxalic acid at a temperature of 7°C and a fixed voltage of 40 V. After the first anodization, the sample was dipped in a solution consisting of a mixture of 0.4 M H₃PO₄ and 0.2 M H₂CrO₄ at 60 °C for 5 h to remove the formed porous film. The second anodization was then carried at 40 V at 7°C in 0.3 M oxalic acid. The pore size of the AAO membranes was widened to about 50 nm using a 5% H₃PO₄ at 30.0 °C for 30min. The first and second anodization lasted respectively 3 h and 8 h. The barrier layer was removed by etching in 5 wt. % H₃PO₄ solution during 50 min at room temperature.

The image J software [34] was used for the estimation of the interpore spacing, pore-size distribution and mean pore diameter as well as to calculate Fast Fourier transforms (FFT) of SEM images.

2.2. Electrochemical deposition of Bi-Te nanowires

The electrolytic solution consisted of Bi₂O₃ and TeO₂ dissolved in a mixture of 1M HNO₃/dimethyl sulfoxide (DMSO) (50% v/v). The pH of the solution was kept at about 1. All the chemicals were of analytical grade and used as received without further purification.

A standard three-electrode electrochemical cell was employed. The cell consisted of a saturated calomel electrode (SCE) reference electrode, an Au-coated AAO template working electrode and a Pt sheet counter electrode. The Au film was deposited by DC-sputtering on one side of the AAO template to provide a conductive contact. The electrodeposition of Bi-Te was performed in the nanopores of the home-made AAO templates using an EGG Potentiostat/Galvanostat Model 273A at room temperature for 1h. The deposition potential was selected from cyclic voltammograms (CVs) recorded at a scan rate of 5 mV/s.

The phase composition and morphology of the Bi₂Te₃ nanowires were characterized by X-ray diffraction analysis (XRD) using a Philips X'Pert MPD diffractometer with Cu K α radiation ($\lambda = 1,5418\text{nm}$) and scanning electron microscope (SEM. JEOL.JSM5500).

3. Results and discussion

3.1. Nanoporous alumina templates

Figure 1.a shows a typical SEM image of the surface of the porous anodic alumina membrane prepared by anodization in 0.3 M oxalic acid solution at a temperature of 7°C and a voltage of 40 V.

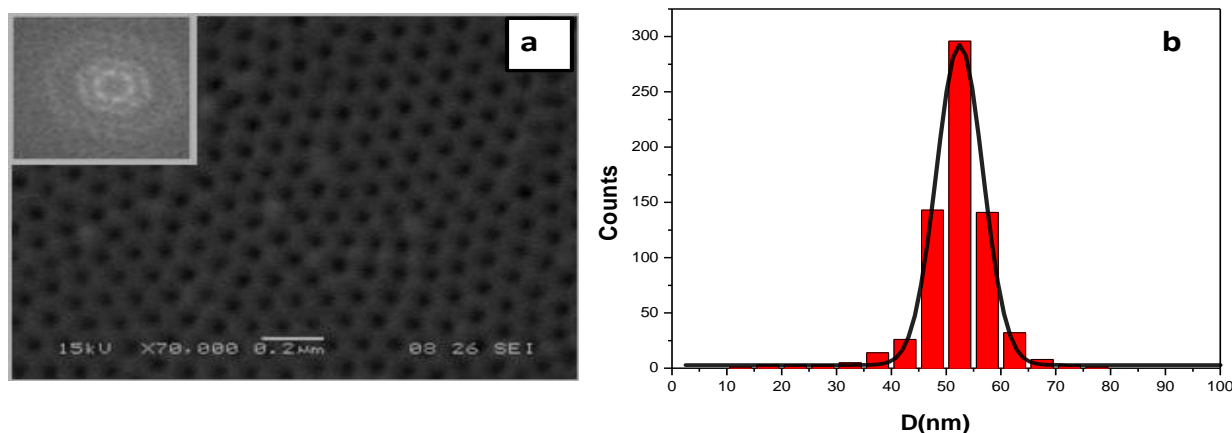
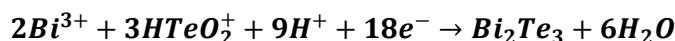


Figure.1:a) SEM images of the surface of an AAO membrane (inset show the FFT of the image), b) Histograms of the pore size distributions for a nanoporous alumina prepared by two-step anodizing at 40 V in 0.3 M oxalic acid at 7 °C.

A hexagonal arrangement of the pores can be clearly seen in the SEM images and in their FFT (inset figure 1-a). The pores are regularly distributed in a honey-comb array which is in agreement with the results reported in the literature [35- 41]. The pore size distributions, depicted in the histograms of Fig.1-b, were evaluated from the measurement of the pore sizes in the image. As reported in details elsewhere [42], the polydispersity of this structure is 8% while the average pore size is ~ 52 nm and the interpore distance is in the range of 100 nm.

3.2. Cyclic voltammetry (CV)

Figure 2 shows the cyclic voltammograms obtained with a small platinum working electrode in a solution containing 1M HNO₃ /dimethyl sulfoxide (DMSO) (50% v/v), 5mM Bi³⁺ and 5mM HTeO₂⁺ with a pH of 1. There is only one pair of reduction/oxidation peaks located at -150 and 500 mV, respectively, which indicates one step reduction mechanism for the deposition of Bi₂Te₃. The reduction peak around -150mV versus SCE is attributed to the following reduction reaction [43]:



Takahashi & al. [44] proposed a mechanism for the deposition of bismuth telluride on Ti substrate: first, the ions migrate from the bulk electrolyte to the electrode surface under the electric field force, and are subsequently adsorbed on the substrate. Second, the adsorbed ions are then reduced to Bi (0) and Te (0) at the cathode. Third, the elemental Te reacted with Bi to form bismuth telluride. Pinisetty D& al. [45] and Jin & al. [46] confirmed the same deposition step on transparent conducting oxide coated glass and Au substrates, respectively.

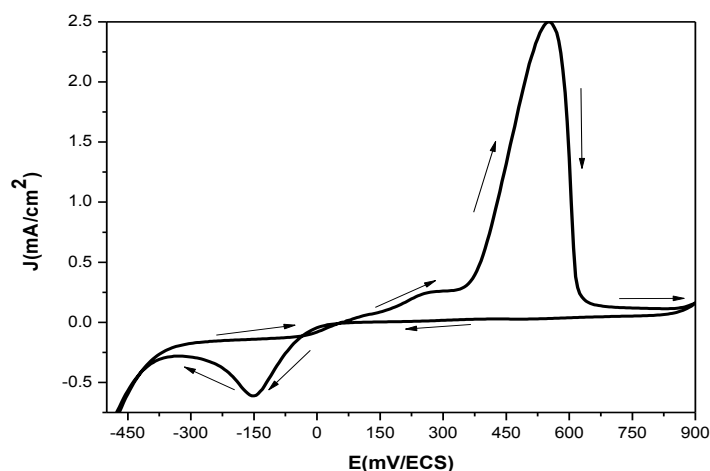


Figure 2: Cyclic voltammograms of platinum electrodes in 1M HNO₃ /dimethyl sulfoxide (DMSO) (50% v/v), 5mM Bi³⁺ and 5mM HTeO₂⁺ at pH~1 at 5mV/s vs. SCE and at room temperature.

3.4. Potentiostatic electrodeposition.

Figure 3 shows the current-time characteristic (chronoamperogram) recorded during the electrodeposition of the Bi-Te nanowires in the nanoporous alumina membrane by applying a potential of -200mV/SCE between the reference electrode and working electrode. Several regions can be distinguished. After a brief transient (region 1) where the pores are empty and nucleation has not yet begun, an almost constant current is observed in region 2; which corresponds to the growth of the nanowires in the pores. This is followed by a sharp increase in the current in regions 3 and 4. This increase is attributed to the overfilling of the pores and the formation of Bi-Te islands on the surface of membrane. This is further supported by the SEM presented below. The onset of this increase in the current corresponds therefore the time required to fill the pores (pore filling time noted *t_d* in Figure 3).

Figure 4 shows the chronoamperogram obtained for two different potentials namely -0.15V and -0.20V vs. SCE. The membranes used for these three samples are identical in thickness and pore size. We note that the cathodic synthesis current, corresponding to the plateau of the characteristic, increases as the potential increases. This behavior is expected because as the potential increases, the current and consequently the deposition rate increase. The filling time, on the other hand, decreases by more than a factor 2 between -0.15V and -0.20V vs. SCE for a pore diameter of about 52 nm.

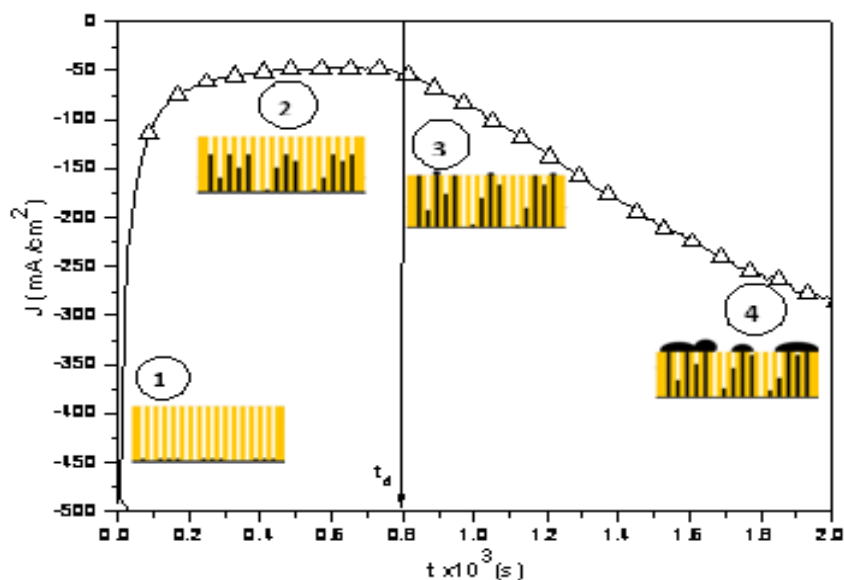


Figure 3: Chronoamperogram characteristic recorded during the synthesis the Bi-Te nanowires in nanoporous alumina membrane at -0.200 Vvs.SCE and at room temperature.

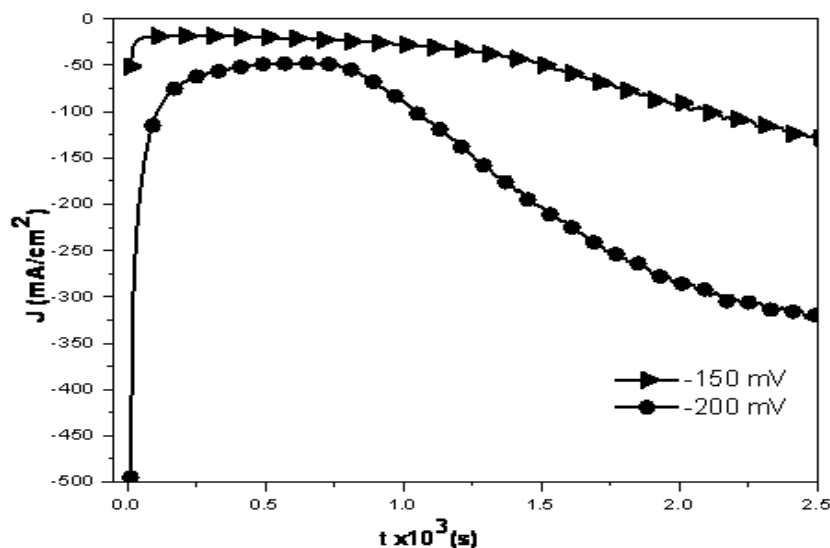


Figure 4: Chronoamperogram characteristic recorded during the synthesis the Bi-Te nanowires in nanoporous alumina membrane at (-0.15, -0.20 Vvs.SCE) and at room temperature.

3.5. Structural and morphological properties of Bi_2Te_3 nanowires

X-ray diffraction pattern of Bi_2Te_3 nanowires formed in the nanoporous alumina is shown in Figure 5. The major diffraction peaks are observed at $2\theta = 27.5^\circ, 38.3^\circ, 40.8^\circ, 50^\circ$ and 57.2° corresponding to (015), (1010), (110), (0015), (205) et (1016) lattice planes of the rhombohedral phase of Bi_2Te_3 (ICDD PDF No.08-00027). No other diffraction peaks of secondary phases, such as the elemental Bi and Te, were detected, indicating that the nanowires are a pure Bi_2Te_3 phase. The crystallite sizes of the nanowires were calculated from the XRD using Scherer's formula [47],

$$D = \frac{k \lambda}{\beta \cos \theta}$$

Where D is the grain size, θ is the diffraction angle, k is the shape factor (0.89), λ is the wavelength of x-ray and β is full width and half maximum (FWHM) of intense peak. The mean crystallite size of Bi_2Te_3 nanowires calculated using Scherer's equation is 30.83 nm.

The SEM images, given in Fig.6(a) and 6(b), show that the nanowires deposited in the AAO templates are densely packed, continuous and extend approximately through the length of each pore. In addition, Islands of Bi_2Te_3 can also be clearly seen on the surface of the of filled AAO nanoporous membrane. The average

diameter of the nanowires is approximately 52 nm, which is equal to the average pore diameter in the AAO template.

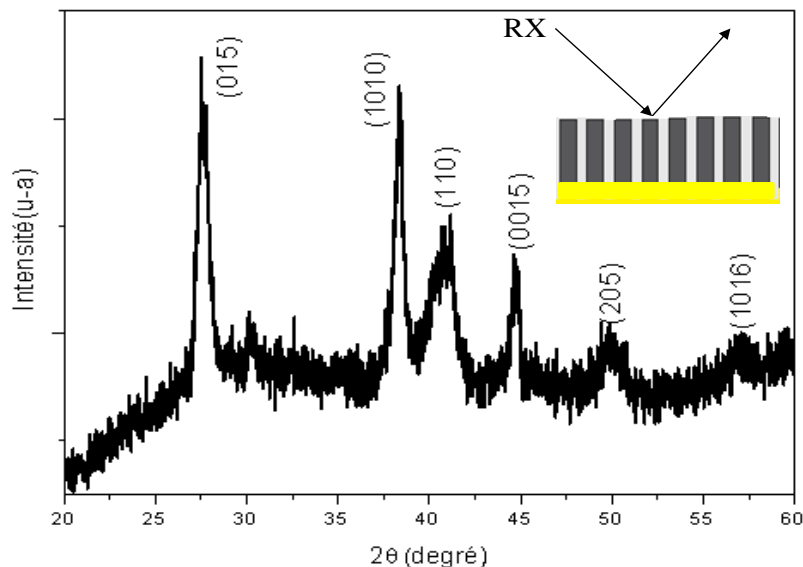


Figure 5: XRD pattern of the obtained Bi_2Te_3 nanowires prepared in 1M HNO_3 /dimethyl sulfoxide (DMSO) (50% v/v), 5mM Bi^{3+} and 5mM HTeO_2^+ at pH~1 ; -0.15 V vs. SCE and at room temperature

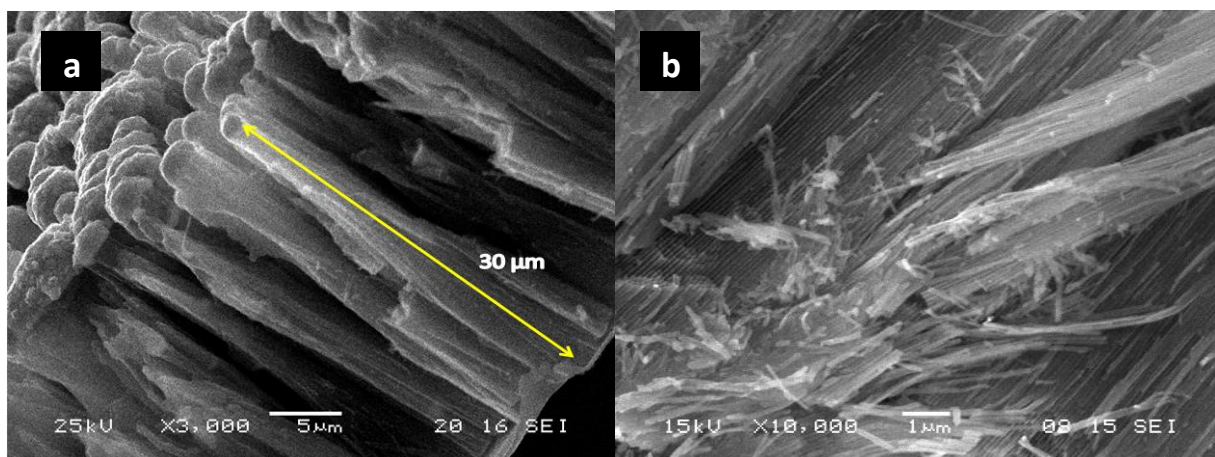


Figure 6: a) Cross section SEM views of the Bi_2Te_3 nanowires electrodeposited in nanoporous alumina membrane at -0.15 V vs. SCE and at room temperature b) SEM image of fractured AAO membrane filled with the nanowires

Conclusion

Bi_2Te_3 nanowires were obtained from a DMSO solution containing 5mM HTeO_2^+ and 5mM Bi^{3+} in nanoporous alumina membrane at -0.200 V vs. SCE. Bi_2Te_3 nanowires with a polycrystalline structure. The crystallite sizes of the nanowires are found to be 30.83 nm.

The SEM images showed dense nanowires extending through the length of the nanopores. The average diameter of the nanowires is approximately 52 nm, which is equal to the average pore diameter in the AAO template.

These results suggest that solution consisting of a mixture of 1M HNO_3 /dimethyl sulfoxide (DMSO) (50% v/v) containing Bi^{3+} and HTeO_2^+ can be used as an alternative to aqueous acidic solutions for Bi_2Te_3 nanowires array deposition in AAO templates, most likely due to the low corrosion and inhibition of H_2 bubble formation in DMSO.

References

1. Patel N.G., Patel P.G., *Solid State Electron.* 35 (1992) 1269.
2. Xiao F., Hangarter C., Yoo B.Y., Rheem Y.W., Lee K.H., Myung N.V., *Electrochim.Acta.* 53 (2008) 8103
3. Omer S.A., Isifield U.G., *Solar Energy Mater. Solar Cell.* 53 (1998) 67.
4. Stolzer M., Stordeur M., Sobita N., Riode V., *Phys. Status Solidi (B).* 138 (1986) 259.

5. Amin F.A.A., Al Ghaffari A.S.S., Issar M.A., Habib A.M., *J. Mater. Sci.* 27 (1992) 1250.
6. Tedenac J.C., Charar S., *Phys. Low Dimens. Struct.* 5–6 (2000) 61.
7. Dresselhaus M.S., Lin Y.M., Koga T., Cronin S.B., Rabin O., Black M.R., Dresselhaus G., *Materials Research*. 71 (2001) 121.
8. Dresselhaus M.S., Lin Y.M., Rabin O., Jorio A., Souza Filho A.G., Pimenta M.A., Saito R., Samsonidze G.G., Dresselhaus G., *J. Mater. Sci. Eng. C* 23 (2003) 129.
11. Vollklein F., Baier V., Dillner U., Kessler E., *Thin Solid Films*. 187 (1990) 253.
12. Charles E., Groubert E., Boyer A., Mater J., *Lett.* 7 (1988) 579.
13. Martin-Lopez R., Lenoir B., Dauscher A., Scherrer H., Scherrer S., *Solid State Commun.* 108 (1998) 285.
14. Jiang J., Chen L., Bai S., Yao Q., Wang Q., *Mater. Sci. Eng. B*. 117 (2005) 334.
15. Okido M., Ichino R., Oyobi Kouon-kagaku Y., *Molten Salts*. 47 (2004) 79.
16. Michel S., Diliberto S., Boulanger C., Stein N., Lecuire J.M., Cryst J., *Growth*. 277 (2005) 274.
17. Miyazaki Y., Kajitani T., Cryst J., *Growth*. 229 (2001) 542.
18. Yang J., Zhu W., Gao X., Bao S., Fan X., *Electroanal. J., Chem.* 577 (2005) 117.
19. Magri P., Boulanger C., Lecuire J.M., Mater J., *Chem.* 6 (1996) 773.
20. Tittes K., Bund A., Plieth W., Bentien A., Paschen S., Plotner M., Gräfe H., Fischer W., *J. Solid State Electrochem.* 7 (2003) 714.
21. Martin C.R., *Science*. 266 (1994) 1961.
22. Fert A., Piraux L., Magn J., *Mat.* 200 (1999) 338.
23. Schönenberger C., van der Zande B. M. I., Fokink L. G. J., Henny M., Schmid C., Krüger M., Bachtold A., Huber R., Birk H., Staufer U., *J. Phys. Chem. B*. 101(1997) 5497.
24. Enculescu I., Sima M., Enculescu M., Enache M., Ion L., Antohe S., Neumann R., *Phys. stat. solidi (b)*. 244, (2007) 1607.
25. Huang L., Wind S.J., O'Brien S.P., *Nano Lett.* 3 (2003) 299.
26. Heo P., Hagiwara K., Ichino R., Okido M., *J. Electrochem. Soc.* 153(4) (2006) C213.
27. Richoux V., Diliberto S., Boulanger C., Lecuire J., *Electrochim. Acta.* 52(9) (2007) 3053.
28. Magri P., Boulanger C., Lecuire J.-M., *J. Mater. Chem.* 6 (1996) 773.
29. Boulanger C., Electron J., *Mater.* 39(9) (2010) 1818.
30. Ma Y., Ahlberg E., Sun Y., Iversen B., Palmqvist A., *Electrochim. Acta.* 56(11) (2011) 4216.
31. Masuda H., Fukuda K., *Science* 268 (1995) 1466.
32. Li F., Zhang L., Metzger R. M., *Chem. Mater.* 10(1998) 2473.
33. Jessensky O., Muller F., Gösele U., *Appl. Phys. Lett.* 72 (1998) 1173.
34. Rasband W.S., *Image J. Edited by Bethesda, Maryland, USA U. S. National Institutes of Health.* 1997–2014.
35. Masuda H., Fukuda K., *Science*. 268 (1995) 1466.
36. Jessensky O., Muller F., Gösele U., *J. Electrochem. Soc.* 145 (1998) 3735.
37. Li F., Zhang L., Metzger R. M., *Chem. Mater.* 10 (1998) 2470.
38. Belwalkar A., Grasing E., Van Geertruyden W., Huang Z., Misiolek W. Z., *J. Memb. Sci.* 319 (2008) 192.
39. Masuda H., Hasegawa F., Ono S., *J. Electrochem. Soc.* 144 (1997) L127.
40. Hwang S.K., Jeong S. H., Hwang H. Y., Lee O. J., Lee K. H., *Korean J. Chem. Eng.* 19 (2002) 467.
41. Jeong S.Y., An M. C., Cho Y. S., Kim D. J., Paek M. C., Kang K. Y., *Curr. Appl. Phys.* 9 (2009) S101.
42. Elyaagoubi M., Najih Y., Khadiri M., Oueriagli A., Outzourhit A., Mabrouki M., *J. Mater. Sci. Eng. B* 5 (2015) 248.
43. Prieto A.L., Sander M.S., Martin-Gonzalez M.S., Gronsky R., Sands T., Stacy A.M., *J. Am. Chem. Soc.* 123 (2001) 7160.
44. Takahashi M., Oda Y., Ogino T., Furuta S., *J. Electrochem. Soc.* 140 (1993) 2550.
45. Pinisetty D., Davis D., Podlaha-Murphy E.J., Murphy M.C., Karki A.B., Young D.P., Devireddy R.V., *Acta Mater.* 59 (2011) 2455.
46. Jin C.G., Xiang X.Q., Jia C., Liu W.F., Cai W.L., Yao L.Z., Li X.G., *J. Phys. Chem. B* 108 (2004) 1844.
47. Warren B.E., *X-ray diffraction, Addison-Wesley Publishing Co, London*, 1969.

(2017) ; <http://www.jmaterenvirosci.com>